The Journal of Engineering

The 9th International Conference on Power Electronics, Machines and Drives (PEMD 2018)

IET Journals
The Institution of Engineering and Technology

Vector control strategies to enable equal frequency operation of the modular multilevel matrix converter

eISSN 2051-3305
Received on 21st June 2018
Accepted on 27th July 2018
E-First on 4th April 2019
doi: 10.1049/joe.2018.8028
www.ietdl.org

Matias Diaz[1] ✉, Mauricio Espinosa[2], Felix Rojas[1], Pat Wheeler[3], Roberto Cardenas[4]

[1]*Electrical Engineering Department, University of Santiago of Chile, Chile*
[2]*Faculty of Engineering, University of Costa Rica, Costa Rica*
[3]*Faculty of Engineering, The University of Nottingham, UK*
[4]*Electrical Engineering Department, University of Chile, Chile*
✉ *E-mail: matias.diazd@usach.cl*

Abstract: The modular multilevel matrix converter (M^3C) is a power converter topology for ac to ac conversion that is suitable for high-power applications. The control of this converter is complex, particularly if ac system frequencies are similar. In these cases, the floating capacitors can present large voltage oscillations. Therefore, this study presents a new vector control system to enable the operation of the M^3C when the frequencies at the input and output are virtually the same. The effectiveness of the proposed method has been validated using simulations and experimental results from a prototype M^3C power converter with 27 cells.

1 Introduction

The modular multilevel matrix converter (M^3C) is a power converter topology for direct ac–ac conversion first proposed for wind energy conversion systems [1]. This power converter has advantages over traditional topologies including modularity, a simple extension to enable operation at high voltage levels with options for redundancy, control flexibility and enhanced waveform quality [2]. Lately, the M^3C has been also proposed for drives [3, 4], large power wind turbines [5, 6] and grid-connected applications [7].

The M^3C is characterised by a cascade connection of full-bridge power cells forming a cluster. The direct ac-to-ac connection of two ac ports is achieved using the nine clusters of the converter, as shown in Fig. 1. The capacitor voltage of each power cell is floating and can charge–discharge during the operation of the converter. Therefore, one of the most important control tasks is to maintain the voltage of each capacitor within an acceptable range [2].

This converter is suitable for low-speed high-power applications because lower circulating currents and common-mode voltage are required to mitigate the oscillations in the capacitors, in comparison to other topologies such as the modular multilevel converter [2]. However, the M^3C has an inherent problem when the frequencies at the input and the output of the converter are very similar or equal. This situation can result in oscillations in the floating capacitor voltages.

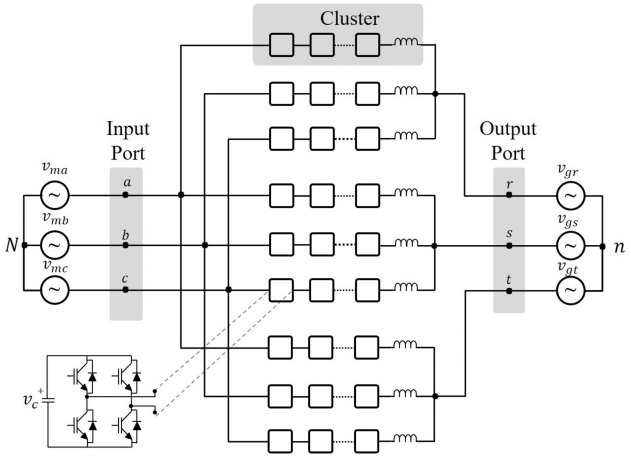

Fig. 1 *Modular multi-level matrix converter topology*

Cascade control systems based on decoupled modelling of the M^3C have been proposed [3, 4]. These previously proposed approaches use circulating currents in the converter along with common-mode voltage control to regulate the voltages across the floating capacitors. When the input-port frequency is low in comparison to the output-port frequency, referred to as low-frequency mode (LFM), the average components of the capacitor voltages are controlled using either the circulating currents or the common-mode voltages [3–6, 8]. When the input-port frequency is close or similar to the output- port frequency, referred to as equal frequencies mode (EFM), mitigation signals are included to compensate the oscillations in the floating capacitor voltages [7, 9]. These mitigation signals are pre-defined offline and can increase the peak current flowing through the converter.

In this context, this paper presents vector control strategies to enable EFM operation of the M^3C. This proposal considers nested control systems to regulate the floating capacitor voltages and the input–output ports. In EFM, circulating currents and common-mode voltage are used to form the mitigation signals that can reduce the oscillations in the floating capacitor voltages to zero. The effectiveness the proposed control strategies is validated through experiment and simulation results from a prototype converter rated at ∼5 kVA with 27 operational cells.

2 Mathematical representation of The M^3C

The dynamics of the M^3C can be represented by a decoupled model obtained using the double $\alpha\beta 0$ transformation [3, 4]. This procedure enables a decoupled representation of the voltages-currents and power-capacitor voltages of the M^3C as follows:

2.1 Voltage-current model of the M^3C

In (1), the representation of the M^3C converter after applying the $\alpha\beta 0$ transformation to both ports of the converter is presented. The model is represented by nine independent equations. Variables v_{xy}, and its associated i_{xy} $x \in \{\alpha, \beta\}$, $y \in \{\alpha, \beta\}$, represent internal cluster voltages of the converter and the so-called circulating

currents. In addition, and as one of the main advantages of this representation, the input and output voltages are decoupled and represented by v_{ij} $i \in \{m, g\}$, $j \in \{\alpha, \beta\}$, respectively. In addition, L_c is a small series inductor in each cluster and v_n represents the common-mode voltage. (see (1))

2.2 Floating capacitor voltage model

Assuming that all power cells of the converter presented in Fig. 1 are equal to C, and their voltages are controlled to v_c^*, the relation of capacitor voltage of each cell and the power of each cluster can be written as [6]

$$Cv_c^*\frac{\mathrm{d}}{\mathrm{d}t}\begin{bmatrix} v_{c_{ar}} & v_{c_{as}} & v_{c_{at}} \\ v_{c_{br}} & v_{c_{bs}} & v_{c_{ct}} \\ v_{c_{cr}} & v_{c_{cs}} & v_{c_{ct}} \end{bmatrix} \simeq \begin{bmatrix} P_{ar} & P_{as} & P_{at} \\ P_{br} & P_{bs} & P_{bt} \\ P_{cr} & P_{cs} & P_{ct} \end{bmatrix} \tag{2}$$

In order to obtain a decoupled representation similar to (1), the $\alpha\beta0$ transform is applied twice to (2), yielding to

$$Cv_c^*\frac{\mathrm{d}}{\mathrm{d}t}\begin{bmatrix} v_{c_{\alpha\alpha}} & v_{c_{\beta\alpha}} & v_{c_{0\alpha}} \\ v_{c_{\alpha\beta}} & v_{c_{\beta\beta}} & v_{c_{0\beta}} \\ v_{c_{\alpha0}} & v_{c_{\beta0}} & v_{c_{00}} \end{bmatrix} \simeq \begin{bmatrix} P_{\alpha\alpha} & P_{\beta\alpha} & P_{0\alpha} \\ P_{\alpha\beta} & P_{\beta\beta} & P_{0\beta} \\ P_{\alpha0} & P_{\beta0} & P_{00} \end{bmatrix} \tag{3}$$

From (3), v_{c0} represents the average voltage present in each cluster, which is calculated based on the net power absorbed/delivered by the converter. The other eight terms represent the voltage imbalances between different clusters and therefore they have to be controlled to be zero.

According to [4], each power term of (3), can be calculated based on the $\alpha\beta0$ components of (1). For instance, $P_{\alpha\alpha}$ yields to

$$\begin{aligned} P_{\alpha\alpha} = {} & \frac{(v_{m\alpha}i_{g\alpha} - v_{g\alpha}i_{m\alpha})}{3} + \frac{(v_{m\alpha}i_{\alpha\alpha} - v_{m\beta}i_{\beta\alpha})}{\sqrt{6}} \\ & - \frac{(v_{g\alpha}i_{\alpha\alpha} - v_{g\beta}i_{\alpha})}{\sqrt{6}} - v_n I_{\alpha\alpha} \end{aligned} \tag{4}$$

Then, replacing (4) into (3)

$$\begin{aligned} \tilde{v}_{c_{\alpha\alpha}} \simeq {} & \frac{V_m I_g \sin(\phi_g + (\omega_g - \omega_m)t) + V_g I_m \sin(\phi_m - (\omega_g - \omega_m)t)}{6Cv_c^*(\omega_g - \omega_m)} \\ & + \frac{V_m I_g \sin(\phi_g + (\omega_g + \omega_m)t) - V_g I_m \sin(\phi_m + (\omega_g + \omega_m)t)}{6Cv_c^*(\omega_g + \omega_m)} \end{aligned} \tag{5}$$

where $\omega_m = 2\pi f_m$ and $\omega_g = 2\pi f_g$. Note that V_m and V_g are the machine and output-port phase-to-neutral peak voltage magnitudes, respectively. I_m and I_g are the machine and output-port peak current magnitudes, respectively. f_m and f_g are the machine and output-port frequencies. The angles ϕ_m and ϕ_g are the machine and output-port phase angles.

Analysing (5), it is possible to conclude that the CCVs can present large voltage oscillations when $f_m = \pm f_g$. The same problem appears in $v_{c_{\alpha\beta}}$, $v_{c_{\beta\alpha}}$ and $v_{c_{\beta\beta}}$ when $f_m = \pm f_g$. Additionally, CCVs $v_{c_{\alpha0}}$ and $v_{c_{\beta0}}$ can lead to large voltage fluctuations when $f_m = 0$ and $v_{c_{0\alpha}}$ and $v_{c_{0\beta}}$ when $f_g = 0$.

2.3 ΣΔ transformation

In order to decouple the voltage oscillation of the cluster capacitors of the circulating terms of (3), a ΣΔ transformation has to be applied to the converter [10, 11]. This transformation also allow a vectorial representation of the internal terms of the converter. Thereby, to transform a generic vector $\vec{X}$ from the double-$\alpha\beta0$ frame to the ΣΔ frame, the following matrix has to be used:

$$\begin{bmatrix} X_{1\alpha}^{\Sigma\Delta} \\ X_{1\beta}^{\Sigma\Delta} \\ X_{2\alpha}^{\Sigma\Delta} \\ X_{2\beta}^{\Sigma\Delta} \end{bmatrix} = \frac{1}{2}\begin{bmatrix} 1 & 0 & 0 & 1 \\ 0 & 1 & -1 & 0 \\ 0 & 1 & 1 & 0 \end{bmatrix}\begin{bmatrix} X_{\alpha\alpha} \\ X_{\alpha\beta} \\ X_{\beta\alpha} \\ X_{\beta\beta} \end{bmatrix} \tag{6}$$

The ΣΔ transformation is applied to (3) yielding to the power-CCV of the M^3C in ΣΔ double-$\alpha\beta0$ coordinates:

$$Cv_c^*\frac{d}{dt}\begin{bmatrix} v_{c_{1\alpha}}^{\Sigma\Delta} & v_{c_{1\beta}}^{\Sigma\Delta} & v_{c_{0\alpha}} \\ v_{c_{2\alpha}}^{\Sigma\Delta} & v_{c_{2\beta}}^{\Sigma\Delta} & v_{c_{0\beta}} \\ v_{c_{\alpha0}} & v_{c_{\beta0}} & v_{c_{00}} \end{bmatrix} \simeq \begin{bmatrix} P_{1\alpha}^{\Sigma\Delta} & P_{1\beta}^{\Sigma\Delta} & P_{0\alpha} \\ P_{2\alpha}^{\Sigma\Delta} & P_{2\beta}^{\Sigma\Delta} & P_{0\beta} \\ P_{\alpha0} & P_{\beta0} & P_{00} \end{bmatrix} \tag{7}$$

The use of the ΣΔ transformation enables a better representation of the CCVs in terms of the ports frequencies because a pair of of CCV ripple terms is obtained for each unstable condition. For example, large voltage oscillations can appear in $\vec{v}_{c_{1\alpha\beta}}^{\Sigma\Delta}$ just when $f_m = f_g$ (and not when $f_m = \pm f_g$ as $v_{c_{\alpha\alpha}}$). Defining the power flows and the cluster capacitor voltages as vectors, the vector power-CCV model in ΣΔ double-$\alpha\beta0$ coordinates can be expressed as follows:

$$\begin{aligned} Cv_c^*\frac{\mathrm{d}\vec{v}_{c_{1\alpha\beta}}^{\Sigma\Delta}}{\mathrm{d}t} \simeq {} & \frac{1}{6}\left(\vec{v}_{m_{\alpha\beta}}^{c}\vec{i}_{g_{\alpha\beta}} - \vec{v}_{g_{\alpha\beta}}\vec{i}_{m_{\alpha\beta}}^{c}\right) \\ & + \frac{1}{\sqrt{6}}\left(\vec{v}_{m_{\alpha\beta}}\vec{i}_{2\alpha\beta}^{\Sigma\Delta} - \vec{v}_{g_{\alpha\beta}}^{c}\vec{i}_{2\alpha\beta}^{\Sigma\Delta^c}\right) - v_n\vec{i}_{1\alpha\beta}^{\Sigma\Delta} \end{aligned} \tag{8}$$

$$\begin{aligned} Cv_c^*\frac{\mathrm{d}\vec{v}_{c_{2\alpha\beta}}^{\Sigma\Delta}}{\mathrm{d}t} \approx {} & \frac{1}{6}\left(\vec{v}_{m_{\alpha\beta}}\vec{i}_{g_{\alpha\beta}} - \vec{v}_{g_{\alpha\beta}}\vec{i}_{m_{\alpha\beta}}\right) \\ & + \frac{1}{\sqrt{6}}\left(\vec{v}_{m_{\alpha\beta}}^{c}\vec{i}_{1\alpha\beta}^{\Sigma\Delta} - \vec{v}_{g_{\alpha\beta}}^{c}\vec{i}_{1\alpha\beta}^{\Sigma\Delta^c}\right) - v_n\vec{i}_{2\alpha\beta}^{\Sigma\Delta} \end{aligned} \tag{9}$$

$$Cv_c^*\frac{\mathrm{d}\vec{v}_{c0}^{\alpha\beta}}{\mathrm{d}t} \simeq \frac{1}{3\sqrt{2}}\left(\vec{v}_{m\alpha\beta}^{c}\vec{i}_{m\alpha\beta}^{c}\right) - \frac{1}{\sqrt{3}}\left(\vec{v}_{g\alpha\beta}\vec{i}_{1\alpha\beta}^{\Sigma\Delta c} + \vec{v}_{g\alpha\beta}^{c}\vec{i}_{2\alpha\beta}^{\Sigma\Delta}\right) - \frac{1}{\sqrt{3}}v_n\vec{i}_{m\alpha\beta} \tag{10}$$

$$Cv_c^*\frac{\mathrm{d}\vec{v}_{c\alpha\beta}^{0}}{\mathrm{d}t} \simeq \frac{-1}{3\sqrt{2}}\left(\vec{v}_{g\alpha\beta}^{c}\vec{i}_{g\alpha\beta}^{c}\right) + \frac{1}{\sqrt{3}}\left(\vec{v}_{m\alpha\beta}\vec{i}_{1\alpha\beta}^{\Sigma\Delta} + \vec{v}_{m\alpha\beta}^{c}\vec{i}_{2\alpha\beta}^{\Sigma\Delta}\right) - \frac{1}{\sqrt{3}}v_n\vec{i}_{g\alpha\beta} \tag{11}$$

The superscript 'c' represents the complex conjugate operator. Equations (8)−(11) represent the vector power-CCV model of the M^3C. This model allows a simple analysis and implementation of vector control structures.

$$\begin{aligned} \sqrt{3}\begin{bmatrix} 0 & 0 & 0 \\ 0 & 0 & 0 \\ v_{m_\alpha} & v_{m_\beta} & 0 \end{bmatrix} = {} & L_c\frac{\mathrm{d}}{\mathrm{d}t}\begin{bmatrix} i_{\alpha\alpha} & i_{\beta\alpha} & i_{0\alpha} \\ i_{\alpha\beta} & i_{\beta\beta} & i_{0\beta} \\ i_{\alpha0} & i_{\beta0} & i_{00} \end{bmatrix} \\ & + \begin{bmatrix} v_{\alpha\alpha} & v_{\beta\alpha} & v_{0\alpha} \\ v_{\alpha\beta} & v_{\beta\beta} & v_{0\beta} \\ v_{\alpha0} & v_{\beta0} & v_{00} \end{bmatrix} + \sqrt{3}\begin{bmatrix} 0 & 0 & v_{g_\alpha} \\ 0 & 0 & v_{g_\beta} \\ 0 & 0 & 0 \end{bmatrix} + \begin{bmatrix} 0 & 0 & 0 \\ 0 & 0 & 0 \\ 0 & 0 & 3v_n \end{bmatrix} \end{aligned} \tag{1}$$

3 Vector control systems of The M^3C

Significant voltage oscillation should be avoided in $\vec{v}^{\Sigma\Delta}_{c1\alpha\beta}$, $\vec{v}^{\Sigma\Delta}_{c2\alpha\beta}$, $\vec{v}^{\alpha\beta}_{c0}$ and $\vec{v}^{0}_{c\alpha\beta}$ when the input–output ports frequencies are close. Notice that, due to the integral effect produced in the capacitors, even small dc components in the powers components of (3) could produce significant voltage imbalances. Consequently, zero steady-state error and good dynamic control of the cluster capacitor voltage unbalances are fundamental to provide proper operation of the converter. Therefore, this proposal considers novel control strategies for decoupled regulation of the CCVs, input-port and the output-port control is proposed. Each control system is described in the following subsections.

3.1 CCVs vector control

Vector control strategies for the regulation of $\vec{v}^{\Sigma\Delta}_{c1\alpha\beta}$, $\vec{v}^{\Sigma\Delta}_{c2\alpha\beta}$, $\vec{v}^{\alpha\beta}_{c0}$, and $\vec{v}^{0}_{c\alpha\beta}$ are proposed. The average value of all the floating capacitor voltages is regulated using the term v_{c00}. In EFM, the CCV vectors are regulated to zero using the last terms of (8)–(11).

It is important to mention that the control of the M^3C in LFM is not included in this paper. However, readers can refer to [4, 6] for more details about the operation of the M^3C in LFM.

3.1.1 Control of the average component of the capacitor voltages: The term v_{c00} represents the average voltage of all the floating capacitors. This term is related to the active power P_{00} flowing into the converter. Therefore, the following expression is written:

$$Cv_c^*\frac{dv_{c00}}{dt} \simeq P_{00} = \frac{\overbrace{v_{m\alpha}i_{m\alpha}+v_{m\beta}i_{m\beta}}^{\text{Input Power} = P_{in}}}{3} - \frac{\overbrace{v_{g\alpha}i_{g\alpha}+v_{g\beta}i_{g\beta}}^{\text{Output Power} = P_{out}}}{3} \tag{12}$$

The term P_{out} represents the M^3C output power which is considered as a disturbance that can be feedforwarded. Additionally, the input-port variables are referred to a dq frame rotating at θ_m and oriented along the grid-voltage. Therefore, (12) becomes

$$Cv_c^*\frac{dv_{c00}}{dt} \simeq P_{00} = \frac{1}{3}v_{md}i_{md} \tag{13}$$

Accordingly, an incremental current $i^*_{md_1}$ can be calculated to regulate the average value of the CCVs using (13)

3.1.2 Control of $\vec{v}^{\Sigma\Delta}_{c1\alpha\beta}$ and $\vec{v}^{\Sigma\Delta}_{c2\alpha\beta}$: The power flows produced by the last terms of (8) and (9) are used to regulate the vectors $\vec{v}^{\Sigma\Delta}_{c1\alpha\beta}$ and $\vec{v}^{\Sigma\Delta}_{c2\alpha\beta}$ when the frequencies are close to $f_m = \pm f_g$.

The voltage oscillations in $\vec{v}^{\Sigma\Delta}_{c1\alpha\beta}$ and $\vec{v}^{\Sigma\Delta}_{c2\alpha\beta}$ are filtered using dq-based filters. Therefore, (8) and (9) yield to

$$Cv_c^*\frac{d\vec{v}^{\Sigma\Delta\,dc}_{c1\alpha\beta}}{dt} \simeq -v_n\vec{i}^{\Sigma\Delta}_{1\alpha\beta} \tag{14}$$

$$Cv_c^*\frac{d\vec{v}^{\Sigma\Delta\,dc}_{c2\alpha\beta}}{dt} \simeq -v_n\vec{i}^{\Sigma\Delta}_{2\alpha\beta} \tag{15}$$

The common-mode voltage and the circulating currents should be in phase to produce adjustable power flows. Therefore, the current references to command $\vec{v}^{\Sigma\Delta}_{1dq}$ and $\vec{v}^{\Sigma\Delta}_{2dq}$ are redefined as follows:

$$\vec{i}^{\Sigma\Delta}_{1\alpha\beta_1} = \vec{I}^{\Sigma\Delta}_{1dq_1}f(t); \quad \vec{i}^{\Sigma\Delta}_{2\alpha\beta_1} = \vec{I}^{\Sigma\Delta}_{2\alpha\beta_1}f(t); \quad v_n = V_0g(t) \tag{16}$$

where $f(t)$ and $g(t)$ are in phase. What is more, $f(t) = A_1\sin\theta_n + A_3\sin 3\theta_n$, where $\theta_n$must be relatively high frequency signal, and $g(t) = \text{sign}\{f(t)\}$. The amplitudes of the constants A_1, A_3 and V_0 are chosen accordingly to the criteria presented in [12]. These definitions imply than $f(t)g(t)$ is mainly dc. Then, (14) and (15) yield to

$$Cv_c^*\frac{d\vec{v}^{\Sigma\Delta_{dc}}_{c1\alpha\beta}}{dt} \simeq -V_0\vec{I}^{\Sigma\Delta}_{1dq1} \tag{17}$$

$$Cv_c^*\frac{d\vec{v}^{\Sigma\Delta_{dc}}_{c2\alpha\beta}}{dt} \simeq -V_0\vec{I}^{\Sigma\Delta}_{2dq1} \tag{18}$$

In EFM, large voltage oscillations can appear in the floating capacitors as the input-port frequency get closer to the output-port frequency. Therefore, additional components of the circulating currents are considered to mitigate these effects. The circulating current references are defined considering the next feedforward components:

$$\vec{I}^{\Sigma\Delta}_{1dq1} = \vec{I}^{\Sigma\Delta}_{1dq1c} + \vec{I}^{\Sigma\Delta}_{1dq1f}; \quad \vec{I}^{\Sigma\Delta}_{1dq1f} = \frac{\left(\vec{v}^{c}_{m_{\alpha\beta}}\vec{i}_{g_{\alpha\beta}} - \vec{v}_{g_{\alpha\beta}}\vec{i}^{c}_{m_{\alpha\beta}}\right)}{6V_0} \tag{19}$$

$$\vec{I}^{\Sigma\Delta}_{2dq1} = \vec{I}^{\Sigma\Delta}_{2dq1c} + \vec{I}^{\Sigma\Delta}_{2dq1f}; \quad \vec{I}^{\Sigma\Delta}_{2dq1f} = \frac{\left(\vec{v}_{m_{\alpha\beta}}\vec{i}_{g_{\alpha\beta}} - \vec{v}_{g_{\alpha\beta}}\vec{i}_{m_{\alpha\beta}}\right)}{6V_0} \tag{20}$$

Finally, using (19) and (20) in (17) and (18):

$$Cv_c^*\frac{d\vec{v}^{\Sigma\Delta_{dc}}_{c1\alpha\beta}}{dt} \simeq -V_0\vec{I}^{\Sigma\Delta}_{1dq1c}; \quad Cv_c^*\frac{d\vec{v}^{\Sigma\Delta_{dc}}_{c2\alpha\beta}}{dt} \simeq -V_0\vec{I}^{\Sigma\Delta}_{2dq1c} \tag{21}$$

The EFM control is presented in Fig. 2. Vectors $\vec{v}^{\Sigma\Delta}_{c1\alpha\beta}$ and $\vec{v}^{\Sigma\Delta}_{c2\alpha\beta}$ are regulated using (21). The voltage oscillation are mitigated using the feedforward components $\vec{I}^{\Sigma\Delta}_{1dq1f}$ and $\vec{I}^{\Sigma\Delta}_{2dq1f}$. The outputs of the external CCV control loops is multiplied by $f(t)$ and the common-mode voltage is imposed as (16).

3.1.3 Control of $\vec{v}^{\alpha\beta}_{c0}$ and $\vec{v}^{0}_{c\alpha\beta}$: Vector $\vec{v}^{\alpha\beta}_{c0}$ can be rewritten as

$$Cv_c^*\frac{d\vec{v}^{\alpha\beta}_{c0}}{dt} \simeq \frac{(\vec{v}_{m_{dq}}\vec{i}_{m_{dq}})e^{-j2\theta_m}}{3\sqrt{2}} - \frac{(\vec{v}_{g_{dq}}\vec{i}^{\Sigma\Delta}_{1dq} + \vec{v}_{g_{dq}}\vec{i}^{\Sigma\Delta}_{2dq})}{\sqrt{3}} \tag{22}$$

Analogously, $\vec{v}^{0}_{c\alpha\beta}$ is expressed as:

$$Cv_c^*\frac{d\vec{v}^{0}_{c\alpha\beta}}{dt} \simeq \frac{-(\vec{v}_{g_{dq}}\vec{i}_{g_{dq}})e^{-j2\theta_g}}{3\sqrt{2}} + \frac{(\vec{v}_{m_{dq}}\vec{i}^{\Sigma\Delta}_{1dq} + \vec{v}_{m_{dq}}\vec{i}^{\Sigma\Delta}_{2dq})}{\sqrt{3}} \tag{23}$$

Being

$$\vec{i}^{\Sigma\Delta}_{1\alpha\beta_2} = \vec{i}^{\Sigma\Delta\,*}_{1dq_2}e^{j\theta_g}; \quad \vec{i}^{\Sigma\Delta}_{2\alpha\beta_2} = \vec{i}^{\Sigma\Delta\,*}_{2dq_2}e^{j\theta_m} \tag{24}$$

In EFM, the voltage oscillations in $\vec{v}^{\alpha\beta}_{c0}$ and $\vec{v}^{0}_{c\alpha\beta}$ are inside an acceptable range and they can be filtered by the capacitors. Therefore, just the average components of the vectors $\vec{v}^{\alpha\beta_{dc}}_{c0}$, $\vec{v}^{0_{dc}}_{c\alpha\beta}$ are regulated using circulating current references inphase with the input-port and the output-port angles:

$$Cv_c^*\frac{d\vec{v}^{\alpha\beta_{dc}}_{c0}}{dt} \simeq -\frac{\vec{v}_{g_{dq}}\vec{i}^{\Sigma\Delta}_{1dq_2}}{\sqrt{3}}; \quad Cv_c^*\frac{d\vec{v}^{0_{dc}}_{c\alpha\beta}}{dt} \simeq -\frac{\vec{v}_{m_{dq}}\vec{i}^{\Sigma\Delta}_{2dq_2}}{\sqrt{3}} \tag{25}$$

The proposed control strategy is presented in Fig. 3. The dc components of the vector $\vec{v}^{\alpha\beta}_{c0}$ are regulated to zero using a power flow in phase with the grid angle θ_g. The same effect is achieved

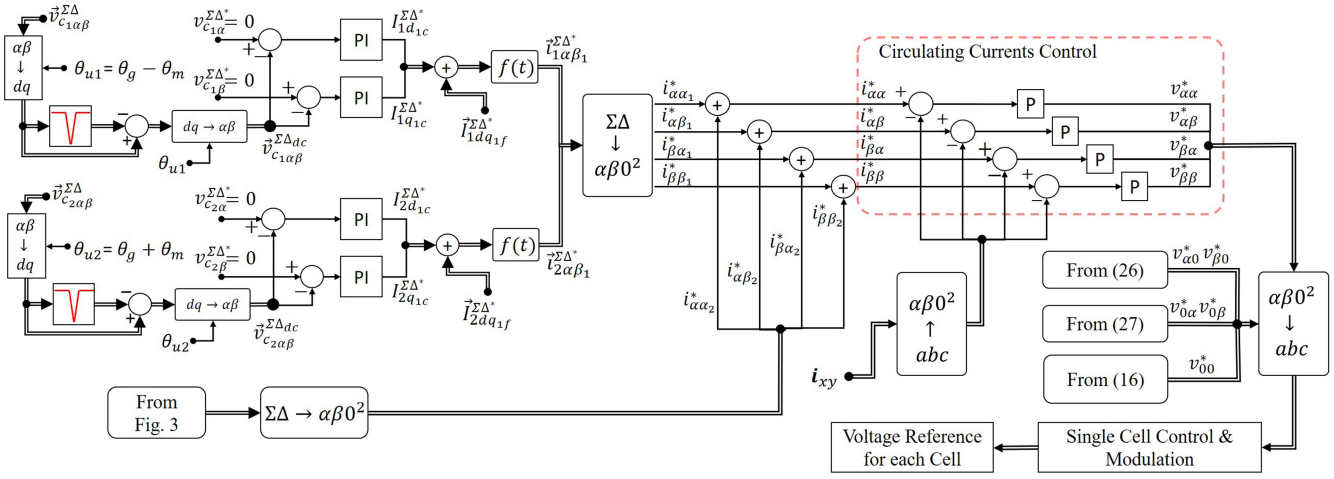

Fig. 2 *Proposed CCV vector control strategy*

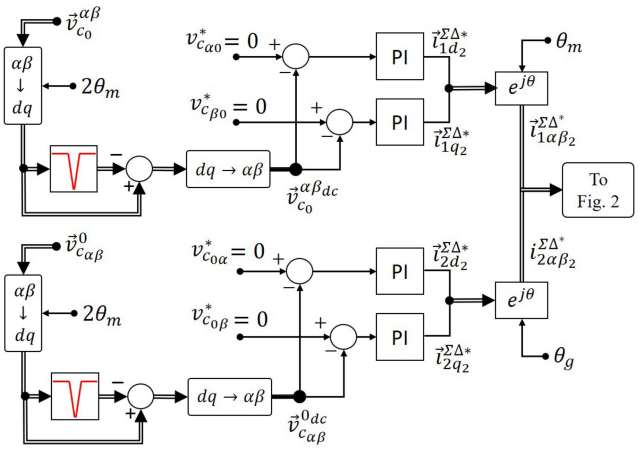

Fig. 3 *Proposed control of* $\vec{v}_{c_0}^{\alpha\beta}$ *and* $\vec{v}_{c_{\alpha\beta}}^{0}$

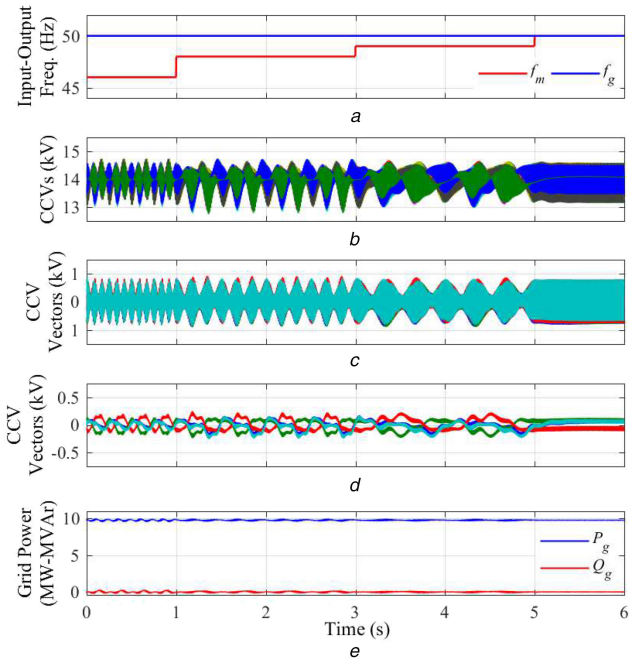

Fig. 4 *Simulation results*

(a) Input and output ports frequencies, ***(b)*** CCVs, ***(c)*** $\vec{v}_{c_0}^{\alpha\beta}$ and $\vec{v}_{c_{\alpha\beta}}^{0}$, ***(d)*** $\vec{v}_{c_{1\alpha\beta}}^{\Sigma\Delta}$ and $\vec{v}_{c_{2\alpha\beta}}^{\Sigma\Delta}$. ***(e)*** Power injected into the grid

for $\vec{v}_{c_{\alpha\beta}}^{0}$ manipulating a non-zero mean active power in phase with the grid angle θ_m.

3.2 Input and output control systems

Using (1), two independent models are obtained for the input and output port dynamics. The dynamics of the input–output ports voltage–current models are controlled using conventional *dq* control systems implemented in *dq* coordinates:

$$\begin{bmatrix} v_{md} \\ v_{mq} \end{bmatrix} = \frac{1}{\sqrt{3}} \begin{bmatrix} v_{d0} \\ v_{q0} \end{bmatrix} + \frac{L_c}{3} \frac{\mathrm{d}}{\mathrm{d}t} \begin{bmatrix} \frac{\mathrm{d}}{\mathrm{d}t} & -\omega_m \\ \omega_m & \frac{\mathrm{d}}{\mathrm{d}t} \end{bmatrix} \begin{bmatrix} i_{md} \\ i_{mq} \end{bmatrix} \tag{26}$$

$$-\begin{bmatrix} v_{gd} \\ v_{gq} \end{bmatrix} = \frac{1}{\sqrt{3}} \begin{bmatrix} v_{0d} \\ v_{0q} \end{bmatrix} + \frac{L_c}{3} \frac{\mathrm{d}}{\mathrm{d}t} \begin{bmatrix} \frac{\mathrm{d}}{\mathrm{d}t} & -\omega_g \\ \omega_g & \frac{\mathrm{d}}{\mathrm{d}t} \end{bmatrix} \begin{bmatrix} i_{gd} \\ i_{gq} \end{bmatrix} \tag{27}$$

The voltage references obtained in (26) and (27) are rotated back to double $\alpha\beta0$ coordinates resulting in $v_{\alpha0}$–$v_{\beta0}$ for the inputport, and $v_{0\alpha}$–$v_{0\beta}$ for the output port. These references are sent to the single-cell control as shown in Fig. 2.

3.3 Single-cell control

The control systems presented in the previous subsections yield to a voltage reference for each cluster in $\alpha\beta0^2$ coordinates. These references are transformed back to the natural reference frame, using the inverse $\alpha\beta0^2$ Transformation, to obtain a voltage reference for each cluster in *abc-rst* coordinates. At this point, additional control loops are used to regulate at the same voltage level all the capacitor voltages within the same cluster. More details about the single-cell control and modulation techniques can be found in [13].

4 Simulation results

A 10 MW M^3C has been implemented in PLECS software to validate the theoretical work proposed in this paper. The simulated M^3C has a nominal power of 10 MW and it features seven power cells per cluster. Each power cell capacitor operates at 2 kV with a capacitance of 7 mF. The outputport is connected to a 6.6 kV 50 Hz ac system, whereas the input port is connected to 5.6 kV variable frequency ac system.

Results for EFM operation are presented in Figs. 4 and 5. The input-port frequency f_m is 46 Hz and it is increased until it reaches 50 Hz, as shown in Fig. 4*a*. The proposed mitigation method is applied as proposed in Fig. 2. Accordingly, the oscillations in $\vec{v}_{c_{1\alpha\beta}}^{\Sigma\Delta}$ are mitigated using the power terms produced by the circulating current and the common-mode voltage. For this test, the common-mode voltage is selected to have an amplitude of 2.5 kV and a fundamental frequency of 120 Hz.

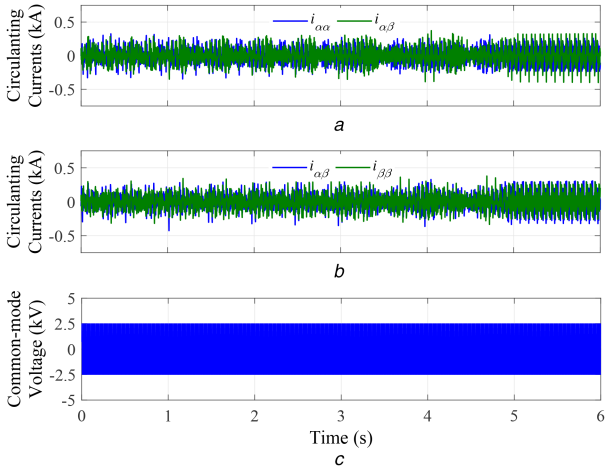

Fig. 5 *Simulation results*
(a) $i_{\alpha\alpha}$ and $i_{\beta\alpha}$, ***(b)*** $i_{\alpha\beta}$ and $i_{\beta\beta}$, ***(c)*** Common-mode voltage

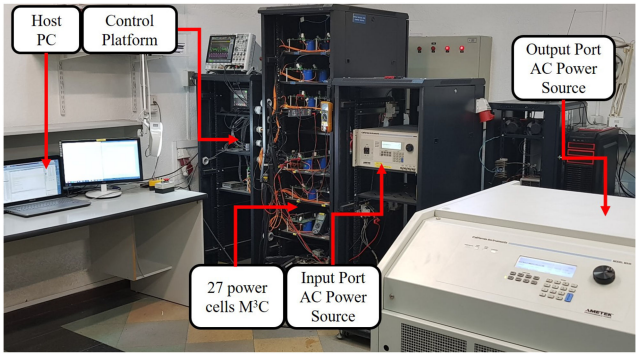

Fig. 6 *Downscaled laboratory prototype*

The CCVs are successfully regulated to 14 kV, as shown in Fig. 4*a*. The vectors $\vec{v}_{c_0}^{\alpha\beta}$ and $\vec{v}_{c_{\alpha\beta}}^{0}$ are presented in Fig. 4*b*, whereas vectors $\vec{v}_{c_{1\alpha\beta}}^{\Sigma\Delta}$ and $\vec{v}_{c_{2\alpha\beta}}^{\Sigma\Delta}$ are presented in Fig. 4*c*. The four vectors are properly regulated to zero and the voltage oscillations are not increased as f_m gets closer to f_g. The active and reactive powers are presented in Fig. 4*d*. Figs. 5*a* and *b* show the circulating currents for this test. The circulating current peak is bounded at the same amplitude than the pre-equal frequency value ≈0.15 kA. This is because the common-mode voltage of Fig. 5*c* is being synthesised to generate manipulable power flows that allow to mitigate the voltage oscillations produced by in EFM.

5 Experimental results

Experimental results have been obtained using an M^3C prototype equipped with 27 cells. A photography of the prototype is shown in Fig. 6. The M^3C comprises a power stage and a control platform. The power stage of the M^3C prototype is composed of nine clusters based on the series connection of three full-H-bridge cells and one inductor. The converter has 27 full-bridge cells connected to a floating capacitor of 4.7 mF. The input and output ports have been connected to Ametek programmable power sources, Model CSW5550 and Model MX45, respectively. The control platform comprises a digital signal processor Texas Instrument board, three field programmable gate array boards, and external boards to provide analogue–digital conversion and computer communication.

In this test, both port frequencies are set to 50 Hz. The common-mode voltage is defined using (16), considering a peak amplitude of 30 V and 120 Hz (fundamental frequency). Moreover, the input-port is set to operate with $P_m = 4$ kW and $Q_m = 0$. The output-port is set with $P_g = 4$ kW and $Q_m = 0$ KVAr.

The 27 capacitor voltages are properly controlled to the desired value ($v_c^* = 150$ V) as shown in Fig. 7*a*. Vectors $\vec{v}_{c_{1\alpha\beta}}^{\Sigma\Delta}$, $\vec{v}_{c_{2\alpha\beta}}^{\Sigma\Delta}$, $\vec{v}_{c_0}^{\alpha\beta}$, $v_{c_{ar1}}$

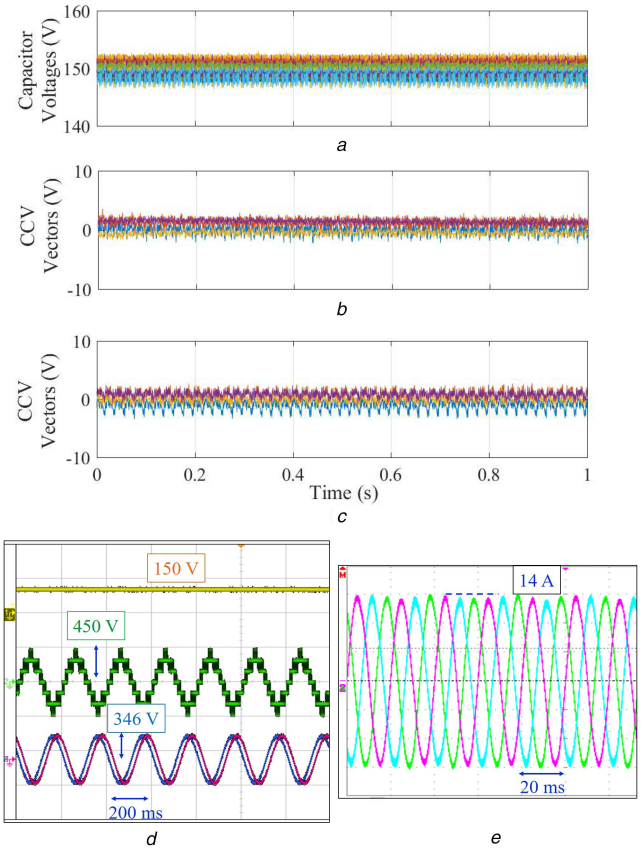

Fig. 7 *Experimental results*
(a) 27 Capacitor voltages, ***(b)*** $\vec{v}_{c_0}^{\alpha\beta}$ and $\vec{v}_{c_{\alpha\beta}}^{0}$, ***(c)*** $\vec{v}_{c_{1\alpha\beta}}^{\Sigma\Delta}$ and $\vec{v}_{c_{2\alpha\beta}}^{\Sigma\Delta}$, ***(d)*** Oscilloscope voltage waveforms, ***(e)*** Oscilloscope output-port current waveform

and $\vec{v}_{c_{\alpha\beta}}^{0}$ are illustrated in Figs. 7*b* and *c*, respectively. For this test, CCV vectors are effectively regulated to zero keeping the ripple below a ± 5 V band.

Oscilloscope waveforms of the voltages and currents of the M^3C are presented. From top to bottom, Fig. 7*d* shows one of the capacitor voltages of the M^3C $v_{c_{ar1}}$, the cluster voltage v_{ar} and the input-output ports voltages $v_{m_{ab}}$ (purple line) and $v_{g_{rt}}$ (blue line). Finally, Fig. 7*e* shows the grid currents which have a peak amplitude of 14 A.

6 Conclusion

This paper proposes vector control strategies to enable the operation of the M^3C in EFM. These strategies are based on the ΣΔ double-$\alpha\beta$0 coordinates representation of the converter, considering the use of the circulating currents and common-mode voltage to mitigate the voltage oscillations in the floating capacitors of the converter.

The proposed control strategies have been discussed and tested through simulations and experiments, which have been conducted using an M^3C equipped with 27 cells. For all tests, the regulation of the input and output ports and the control of the oscillations in the floating capacitor voltages have presented accurate performance.

7 References

[1] Erickson, R., Angkititrakul, S., Almazeedi, K.: 'A new family of multilevel matrix converters for wind power applications: final report'. Tech. Rep., University of Colorado, December, 2006

[2] Okazaki, Y., Kawamura, W., Hagiwara, M., *et al.*: 'Which is more suitable for MMCC-based medium-voltage motor drives, a DSCC inverter or a TSBC converter?'. 9th Int. Conf. on Power Electronics ECCE Asia: 'Green World with Power Electronics', Seoul, South Korea, June 2015, pp. 1053–1060

[3] Kammerer, F., Kolb, J., Braun, M.: 'Fully decoupled current control and energy balancing of the modular multilevel matrix converter'. 15th Int. Power Electronics and Motion Control Conf. and Exposition, EPE-PEMC 2012 ECCE Europe, Novia Sad, Serbia, September 2012, pp. LS2a.3-1–LS2a.3-8

[4] Kawamura, W., Hagiwara, M., Akagi, H.: 'Control and experiment of a modular multilevel cascade converter based on triple-star bridge cells', *IEEE Trans. Ind. Appl.*, 2014, **50**, (5), pp. 3536–3548

[5] Díaz, M., Cárdenas, R., Mauricio Espinoza, B., *et al.*: 'A novel LVRT control strategy for modular multilevel matrix converter based high-power wind energy conversion systems'. 2015 10th Int. Conf. on Ecological Vehicles and Renewable Energies, EVER 2015, Monte Carlo, Monaco, March 2015, pp. 1–11

[6] Diaz, M., Cardenas, R., Espinoza, M., *et al.*: 'Control of wind energy conversion systems based on the modular multilevel matrix converter', *IEEE Trans. Ind. Electron.*, 2017, **64**, (11), pp. 1–1

[7] Fan, B., Wang, K., Wheeler, P., *et al.*: 'A branch current reallocation based energy balancing strategy for the modular multilevel matrix converter operating around equal frequency', *IEEE Trans. Power Electron.*, 2018, **33**, (2), pp. 1105–1117

[8] Diaz, M., Cárdenas, R., Espinoza, M., *et al.*: 'Modelling and control of the modular multilevel matrix converter and its application to wind energy conversion systems'. IECON 2016 42nd Annual Conf. of the IEEE Industrial Electronics Society, no. 1140337, Firenze, Italy, October 2016, pp. 5052–5057

[9] Kawamura, W., Chiba, Y., Hagiwara, M., *et al.*: 'Experimental verification of an electrical drive fed by a modular multilevel TSBC converter when the motor frequency gets closer or equal to the supply frequency', *IEEE Trans. Ind. Appl.*, 2017, **53**, (3), pp. 1–1

[10] Espinoza, M., Cárdenas, R., Díaz, M., *et al.*: 'Modelling and control of the modular multilevel converter in back to back configuration for high power induction machine drives'. IECON Proc. (Industrial Electronics Conf.), October 2016, pp. 5046–5051

[11] Kammerer, F., Gommeringer, M., Kolb, J., *et al.*: 'Energy balancing of the modular multilevel matrix converter based on a new transformed arm power analysis'. 2014 16th European Conf. on Power Electronics and Applications, EPE-ECCE Europe 2014, Lappeenranta, Finland, August 2014, pp. 1–10

[12] Espinoza, M., Espina, E., Diaz, M., *et al.*: 'Improved control strategy of the modular multilevel converter for high power drive applications in low frequency operation'. 2016 18th European Conf. on Power Electronics and Applications (EPE'16 ECCE Europe), Karlsruhe, Germany, September 2016, pp. 1–10

[13] Akagi, H., Inoue, S., Yoshii, T.: 'Control and performance of a transformerless cascade PWM STATCOM with star configuration', *IEEE Trans. Ind. Appl.*, 2007, **43**, (4), pp. 1041–1049